Hot Deformation Mechanisms in a Powder Metallurgy Nickel-Base Superalloy IN 625

S.C. MEDEIROS, W.G. FRAZIER, and Y.V.R.K. PRASAD

The hot working behavior of the nickel-base superalloy IN 625 produced by hot extrusion of a powder metallurgy (P/M) compact has been studied by compression testing in the temperature range 900 °C to 1200 °C and true strain rate range 0.001 to 100 s^{-1}. At strain rates less than about 0.1 s^{-1}, the stress-strain curves exhibited near steady-state behavior, while at higher strain rates, the flow stress reached a peak before flow softening occurred. The processing maps developed on the basis of the temperature and strain rate and strain dependence of the flow stress exhibited three domains. (1) The first domain occurs at lower strain rates (<0.01 s^{-1}) and temperatures higher than about 1050 °C. The peak efficiency and the temperature at which it occurs have increased with strain. The microstructure of the specimen deformed in this domain exhibited extensive wedge cracking. (2) The second domain occurs in the intermediate range of strain rates (0.01 to 0.1 s^{-1}) and temperatures lower than 1050 °C, and in this domain, microstructural observations indicated dynamic recrystallization (DRX) of γ containing δ precipitates and carbide particles resulting in a fine-grained structure. (3) The third domain occurs at higher strain rates (>10 s^{-1}) and temperatures above 1050 °C, with a peak efficiency of about 42 pct occurring at 1150 °C and 100 s^{-1}. Microstructural observations in this domain revealed features such as irregular grain boundaries and grain interiors nearly free from annealing twins, which are typical of DRX of homogeneous γ phase. The instability map revealed that flow instability occurs at strain rates above 1 s^{-1} and temperatures below 1050 °C, and this is manifested as intense adiabatic shear bands. These results suggest that bulk metal working of this material may be carried out in the high strain rate domain where DRX of homogeneous γ occurs. On the other hand, for achieving a fine-grained product, finishing operations may be done in the intermediate strain rate domain. The wedge cracking domain and the regime of instability must be totally avoided for achieving defect-free products.

I. INTRODUCTION

THE nickel-base superalloy IN 625* possesses an attractive combination of properties such as high strength, corrosion resistance,[1] and fatigue strength, for which it is picked commonly in a sheet form by the designers of gas turbine engines, heat exchangers, and reaction vessels. Its high-temperature strength is achieved primarily by solid solution strengthening of nickel by iron, molybdenum, and niobium. However, by increasing the aluminum and titanium contents in the alloy, a special age hardenable grade is manufactured.[2] Since it is required mostly in a sheet form, considerable mechanical processing is involved in its manufacture, which includes several stages of hot working followed by a few steps of cold rolling for achieving additional strength, dimensional accuracy, and surface finish. For the design and optimization of hot working processes and for microstructural control, studies on the evaluation of the hot deformation behavior will be very useful. Zhao *et al.*[3] recently studied the flow behavior of three different commercially available types of IN 625 alloys during hot deformation. On the basis of a detailed microstructural study, the temperature and strain rate conditions for DRX, and partial to complete recrystallization, have been established. In the microstructure of IN 625 alloy, several microstructural phases are present, which include Ni_3Nb (δ) precipitates, Laves phases, and complex carbides such as MC, M_6C, and $M_{23}C_6$. The alloy is usually solutionized at 1100 °C, where all phases except the carbides go into solution.[4]

The aim of the present investigation is to study the mechanisms of hot deformation in IN 625 over a wide range of temperature and strain rate regimes so that these may be explored for optimizing bulk metal working processes such as rolling, forging, or extrusion. The IN 625 alloy investigated has been produced by a powder metallurgy (P/M) route, which gives the advantages of reducing segregation of alloying elements, distributing the carbides and other microconstituents more uniformly in the matrix, and producing finer grain sizes. It is generally recognized that the prior processing history has a significant influence on the hot deformation behavior, and therefore, this study will provide an opportunity to compare the hot deformation behavior of the P/M product with the conventionally produced material.

In this study, the approach of processing maps has been adopted to represent and analyze the constitutive behavior of IN 625 during hot deformation. The basis and principles

* IN 625 is a trademark of INCO Alloys International, Inc., Huntington, WV.

S.C. MEDEIROS, Materials Research Engineer, and W.G. FRAZIER, Research Leader, are with the Materials Process Design Branch, Manufacturing Technology Division, Materials and Manufacturing Directorate, Air Force Research Laboratory, Wright-Patterson Air Force Base, OH 45433-7746. Y.V.R.K. PRASAD, formerly NRC Research Associate, Materials Process Design Branch, Manufacturing Technology Division, Materials and Manufacturing Directorate, Air Force Research Laboratory, is Professor, Department of Metallurgy, Indian Institute of Science, Bangalore 560012, India.

Manuscript submitted August 30, 1999.

of this approach have been described earlier,[5] and its application to the hot working of a wide range of materials has been compiled recently.[6] In brief, depicted in a frame of temperature and strain rate, power dissipation maps represent the pattern in which power is dissipated by the material through microstructural changes. The rate of this change is given by the dimensionless parameter called the efficiency of power dissipation:

$$\eta = \frac{2m}{m + 1} \qquad [1]$$

where m is strain rate sensitivity of flow stress. Over this frame is superimposed a continuum instability criterion for identifying regimes of flow instabilities, developed on the basis of extremum principles of irreversible thermodynamics as applied to large plastic flow[7] and given by another dimensionless parameter:

$$\xi(\dot{\varepsilon}) = \frac{\partial \ln (m/m + 1)}{\partial \ln \dot{\varepsilon}} + m < 0 \qquad [2]$$

where $\dot{\varepsilon}$ is the applied strain rate. Flow instabilities are predicted to occur when $\xi(\dot{\varepsilon})$ is negative. These two maps together constitute a processing map, which exhibits domains with local efficiency maxima representing certain specific microstructural mechanisms together with regimes of flow instabilities.

II. EXPERIMENTAL

The chemical composition (wt pct) of the IN 625 alloy was as follows: Ni-62.6, Cr-19.9, Mo-9.2, Nb-3.81, Fe-2.99, Al-0.20, Ti-0.16, Co-0.10, C-0.02, Mn-0.05, and S-0.002. Argon atomized powder of −100 mesh size was canned in a stainless steel container, hot-isostatically pressed at 1120 °C and 103 MPa for 12 hours, and extruded through a rectangular die. The material had 100 pct theoretical density. Cylindrical compression specimens of 10mm diameter x 15-mm height were machined from the extruded slab in such a fashion that the compression axis of the specimen was along the short transverse direction of the slab. Hot compression tests were conducted in the temperature range 900 °C to 1200 °C at 50 °C intervals and constant true strain rate range of 0.001 to 100 s^{-1} at intervals of an order of magnitude. During testing, the actual temperature of the specimen as well as the adiabatic temperature rise were measured using a thermocouple inserted in a 1-mm hole machined to reach the center of the specimen at half its height. The specimens were coated with a borosilicate glass paste, which acted as a lubricant and also protected the specimen from excessive oxidation. All specimens were deformed to half their height and air-cooled to room temperature following deformation.

The true stress-true strain curves were then determined from the resulting load stroke data. The flow stress data at different temperatures and strain rates were then used to compute the power dissipation efficiency parameter (η) as given by Eq. [1]. A power dissipation map was developed by plotting the variation of efficiency with temperature and strain rate. Regimes of flow instability were delineated using the continuum criterion as given in Eq. [2].

The deformed specimens were sectioned parallel to the compression axis and prepared for metallographic examination using standard procedures. The polished specimens were etched by immersion in a solution containing 50 mL H_2O + 50 mL HCl + 10 ml HF + 3 mL H_2O_2.

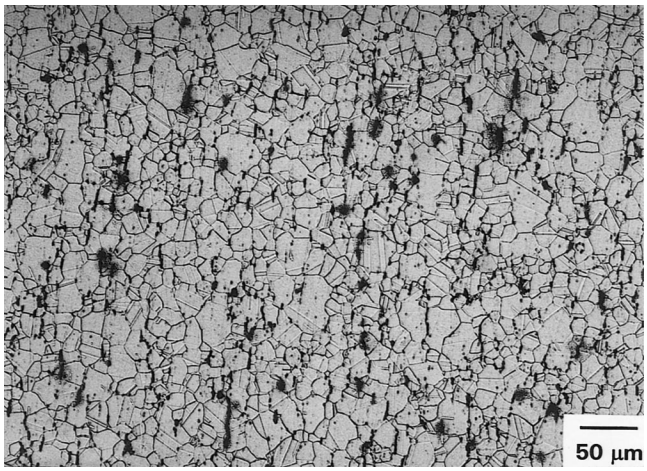

Fig. 1—Initial microstructure of IN 625 in extruded condition. The extrusion direction is vertical.

III. RESULTS AND DISCUSSION

A. *Initial Microstructure*

The microstructure of as-received material is shown in Figure 1, which consists of fine-equiaxed γ grains, annealing twins, and carbides aligned in the extrusion direction, which is vertical in the figure. The average grain diameter is estimated to be about 13 μm. It may be mentioned here that the microstructure did not reveal the presence of any prior particle boundaries that might have been removed by the hot extrusion process.

B. *Stress-Strain Behavior*

Representative true stress–true strain curves obtained at various strain rates and at temperatures below about 1000 °C are shown in Figure 2(a), which corresponds to a temperature of 950 °C. Those obtained at higher temperatures (above 1050 °C) are shown in Figure 2(b), which corresponds to a temperature of 1150 °C. The shapes of the stress-strain curves are similar to those reported earlier by Zhao *et al.*[3] Referring to Figures 2(a) and (b), it may be observed that at strain rates lower than about 0.01 s^{-1}, the stress - strain curves are of steady-state type at all temperatures, while those at temperatures lower than 1050 °C exhibited initial yield drops before a steady state is reached (Figure 2(a)). At strain rates higher than 0.1 s^{-1} and at temperatures lower than 1000 °C, the material initially work hardens and the strain at which the flow stress reaches a peak is lower at lower strain rates. The rate of work hardening, however, is not very sensitive to the strain rate. At temperatures beyond 1050 °C, however, the strain to reach the peak flow stress is lower at lower strain rates as well as at higher temperatures. These differences clearly show that the flow behavior is changing across a characteristic temperature of about 1050 °C and strain rates between 0.1 to 1.0 s^{-1}. It may be noted that this characteristic temperature is close to that at which all the precipitates except carbides go into solution.[4] The

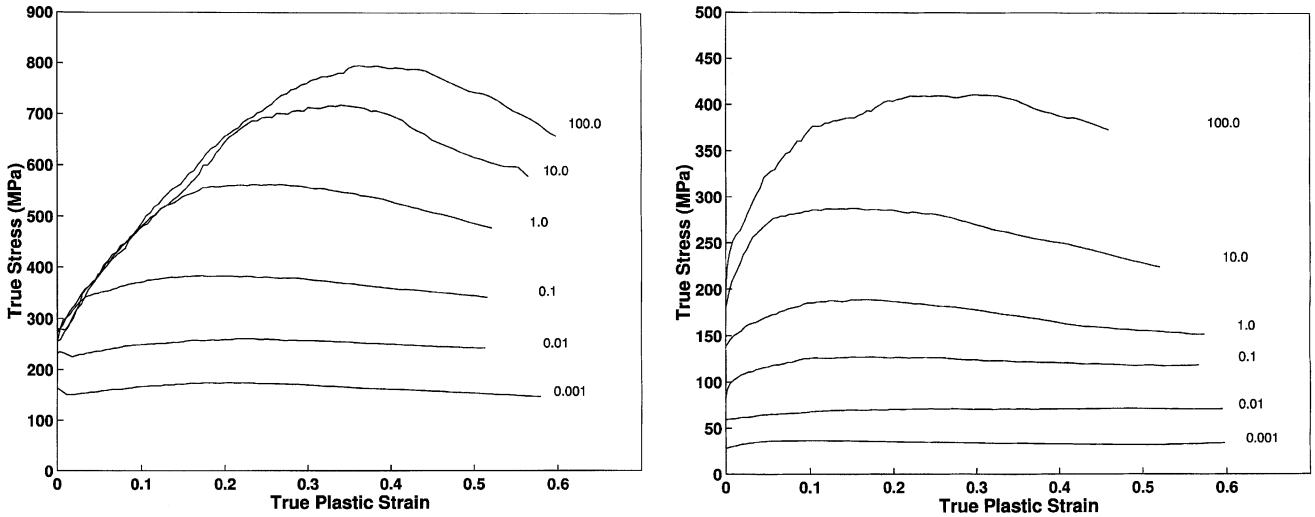

Fig. 2—True stress–true plastic strain curves of IN 625 obtained at (*a*) 950 °C and (*b*) 1150 °C at different strain rates (expressed in s^{-1}).

Table I. Flow Stress Data (in MPa) of IN-625 at Different Temperatures, Strain Rates, and Strains, Corrected for Adiabatic Temperature Rise

Strain	Strain Rate s^{-1}	Temperature, °C						
		900	950	1000	1050	1100	1150	1200
0.1	0.001	222.3	165.7	110.8	71.4	53.0	36.5	25.4
	0.010	302.0	249.0	180.6	128.7	93.5	67.2	39.5
	0.100	514.4	402.5	293.8	208.1	156.6	125.4	84.2
	1.000	498.0	483.7	454.2	317.4	240.9	185.3	145.8
	10.00	512.7	493.0	475.5	455.4	362.1	284.5	241.9
	100.0	533.4	505.6	481.2	458.4	471.2	414.3	328.3
0.2	0.001	235.6	172.8	110.6	74.2	53.2	35.4	25.6
	0.010	312.0	258.7	184.7	131.4	96.4	70.5	48.3
	0.100	536.4	416.3	295.6	211.3	158.7	126.3	89.6
	1.000	717.6	611.5	496.6	322.0	245.7	186.8	145.1
	10.00	738.9	690.3	648.3	507.7	380.2	286.0	239.1
	100.0	706.9	682.6	660.9	613.8	570.3	463.7	354.5
0.3	0.001	237.2	169.6	106.2	72.4	52.2	34.0	24.3
	0.010	304.0	257.4	179.2	126.9	93.7	70.4	49.9
	0.100	551.9	412.7	278.8	204.5	151.9	124.3	88.5
	1.000	836.6	645.3	480.8	308.7	232.2	178.1	136.6
	10.00	980.6	836.5	722.5	499.5	364.6	269.9	226.8
	100.0	896.5	830.8	774.5	686.9	588.9	474.0	339.1
0.4	0.001	235.6	160.9	103.3	72.0	50.4	33.0	23.2
	0.010	291.8	249.9	171.4	121.0	91.9	71.1	49.2
	0.100	545.0	396.9	264.0	191.1	145.6	120.8	88.1
	1.000	805.9	616.3	448.2	288.9	217.7	164.8	131.4
	10.00	1099.0	877.1	712.5	482.0	335.7	250.8	213.5
	100.0	1066.2	929.0	818.2	683.2	558.9	450.2	306.8
0.5	0.001	233.0	153.9	103.1	72.4	48.7	31.8	22.9
	0.010	278.7	242.8	165.5	117.1	90.4	71.4	47.6
	0.100	525.6	382.1	256.1	182.0	139.4	118.2	86.2
	1.000	748.9	568.4	416.2	264.3	205.2	155.5	128.5
	10.00	1214.4	865.4	633.3	429.0	302.9	229.0	200.7
	100.0	1040.3	891.1	772.7	633.1	492.7	413.2	272.4

impact of this temperature on the deformation behavior gets further revealed if the data are analyzed explicitly in terms of processing maps, as discussed subsequently. The flow stress data, corrected for the adiabatic temperature rise, are given in Table I as a function of temperature, strain rate, and strain.

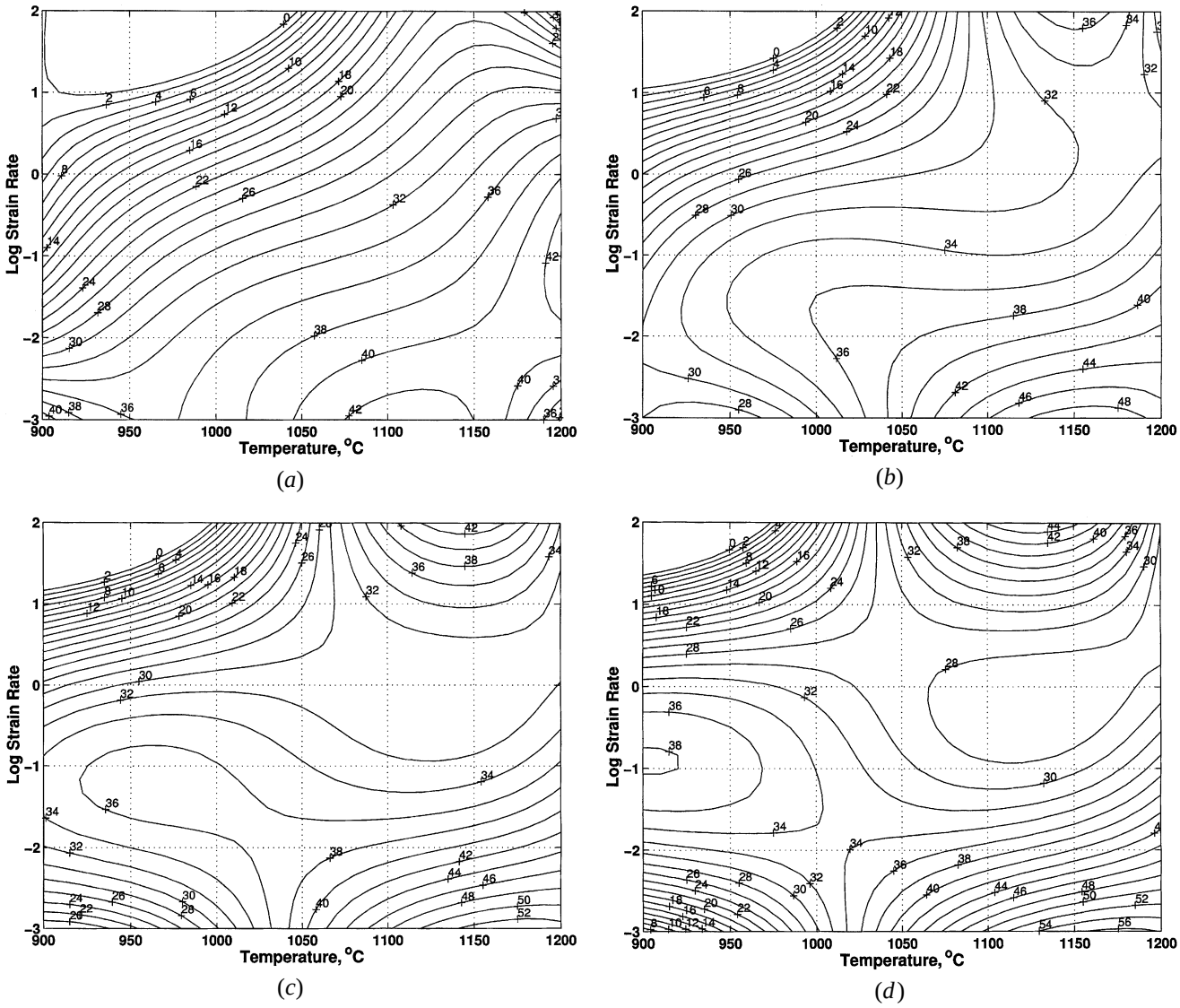

Fig. 3—Power dissipation map obtained on IN 625 at a strain of (*a*) 0.1, (*b*) 0.2, (*c*) 0.3, and (*d*) 0.5. The contours represent isoefficiency of power dissipation expressed in pct.

C. *Power Dissipation Maps*

The power dissipation maps developed at strains of 0.1, 0.2, 0.3, and 0.5, on the basis of the flow stress data given in Table I, are shown in Figures 3(a) through (d), respectively. The power dissipation maps show isoefficiency contours, which represent the relative rate of entropy production occurring in the material due to microstructural dissipation.[6] The map obtained at a strain of 0.1 (Figure 3(a)) exhibits only one domain (called lower strain rate domain) at a temperature of 1100 °C and a strain rate of 0.001 s^{-1} with a maximum efficiency of power dissipation of about 44 pct. As the strain increases, this domain moves toward higher temperatures and its peak efficiency increases to about 57 pct (Figures 3(b) through (d)). At the same time, two different domains start appearing in the maps at higher strains.

(1) At intermediate strain rates (0.01 to 0.1 s^{-1}) and in the temperature range 900 °C to 1050 °C, the contours are getting organized at a strain of 0.2 (Figure 3(b)) and the domain becomes clear beyond a strain of 0.3 (Figures 3(c) and (d)). This domain has a characteristic peak efficiency of about 37 pct occurring at about 950 °C and 0.05 s^{-1}.

(2) At higher strain rates (>10 s^{-1}) and temperatures higher than 1050 °C, a second domain starts to appear in the map at a strain of 0.2 with a peak efficiency of about 37 pct at 1150 °C and 100 s^{-1} (Figure 3(b)). This higher strain rate domain gets developed further at higher strains and the peak efficiency increases to about 43 pct at a strain of 0.5 (Figure 3(d)). However, the temperature and strain rate conditions for the peak efficiency remained unchanged.

The microstructural mechanisms corresponding to the preceding three domains are identified and correlated with the flow behavior in the following section.

1. *Lower strain rate domain*

The lower strain rate and higher temperature domain has a high efficiency of power dissipation (>50 pct), which has increased with increasing strain. Also, the domain started

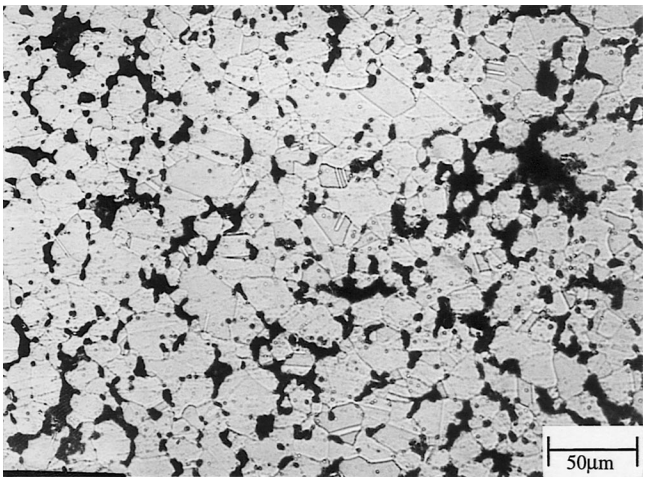

Fig. 4—Microstructure of IN 625 specimen deformed at 1200 °C and 0.001/s showing extensive wedge cracking. The micrograph was obtained in the bulge region of the compression specimen.

Fig. 5—Microstructure of IN 625 specimen deformed at 950 °C and 0.1/s exhibiting a fine grain DRX microstructure.

to appear at a lower strain, suggesting that the transient to form this domain is shorter. At higher temperatures and lower strain rates, the most probable mechanism of deformation is the sliding of grain boundaries,[8] which will significantly contribute to the total strain when the material is fine grained. The consequences of the grain boundary sliding process depend upon the accommodation mechanism at the grain boundary triple junctions, where there will be considerable stress concentration caused by the sliding of two of the neighboring grains. If the stress concentration is accommodated by diffusional flow of matter at rates matching the rate of grain boundary sliding, superplasticity will result.[9] Otherwise, wedge cracking will occur, which may ultimately result in an intercrystalline fracture under a tensile state of stress. However, when the deformation is under an uniaxial compression, steady-state stress-strain curves will be observed (Figure 2(b)), since wedge cracking does not propagate quickly. The microstructure of the specimen deformed at 1200 °C and 0.001 s^{-1} is shown in Figure 4, which clearly revealed extensive wedge cracking in the bulge region of the specimen, where there is tensile hoop stress. Since the grain boundary sliding occurs right from the start of the deformation, it has a shorter transient and the domain will start appearing early in strain. As the strain increases, there is a possibility for the occurrence of grain growth, which moves the efficiency peak in the domain to higher temperatures. Also, at higher temperatures, the domain is likely to close at a faster rate due to an increased rate of grain growth reducing the grain boundary area and restricting the sliding process. Thus, it may be concluded that the lower strain rate domain represents a wedge cracking mechanism, which causes microstructural damage and reduces the hot workability drastically. A tensile test was performed on a cylindrical specimen of the material (gage length = 25 mm) at 1200 °C and a nominal strain rate of 0.001 s^{-1} (cross head speed of 0.25 mm/s), and the total elongation measured was only about 10 pct. In view of the poor workability associated with this domain, it must be strictly avoided in designing metal working processes for this material.

2. *Intermediate strain rate domain*

The domain occurring at intermediate strain rates (0.01 to 0.1 s^{-1}) and in the temperature range 900 °C to 1050 °C has a peak efficiency of about 37 pct. Domains with such a peak efficiency in nickel-base superalloys represent DRX.[6] A small amount of flow softening in the stress - strain curves is observed under these conditions (Figure 2(a)). It may be noted that below 1050 °C, the γ matrix will have δ (Ni_3Nb) precipitates and carbides, which not only assist in nucleating DRX but also restrict the grain boundary migration, such that a fine-grained microstructure results after deformation. The microstructure of the specimen deformed at 950 °C and 0.1 s^{-1} is shown in Figure 5, which confirms the preceding interpretation. Similar microstructures are also observed in IN718 superalloy[10,11] but at lower strain rates (0.001 s^{-1}). Thus, it may be concluded that this intermediate strain rate domain represents DRX of γ occurring in the presence of precipitate and carbide particles. In view of the fine-grained structures that are generated by deformation in this domain, it may be preferred to conduct finish forming operations.

3. *Higher strain rate domain*

The domain at higher strain rates (>10 s^{-1}) starts appearing at a strain of 0.2 and is fully developed at larger strains. Such a strain dependence suggests that the mechanism representing this domain has a higher time constant for the transient. During this stage, nucleation of the process occurs, and at larger strains, the process reaches a steady state. The peak efficiency of power dissipation in this domain is about 42 pct. It may be noted that this domain occurs at temperatures beyond the solutionizing temperature, where all the precipitates have gone into solution. A domain with a similar efficiency has also occurred in IN 718 superalloy[10] at a temperature beyond the solutionizing temperature, which was identified to represent DRX of γ of that alloy. The microstructures of IN 625 specimen deformed at 1100 °C, 1150 °C, and 1200 °C and 100 s^{-1} are shown in Figures 6(a) through (c), which exhibit features that are typical of DRX. These include wavy or irregular grain boundaries and grain interiors, that are nearly free from annealing twins. Further, the shape of the stress - strain curves (Figure 2(b)) observed under conditions in this domain support this interpretation, since they exhibit flow stress peaks followed by flow softening, which is typical of materials that undergo DRX.[12] Also, the critical strain (for the peak flow stress) is higher for higher strain rates and lower temperatures as

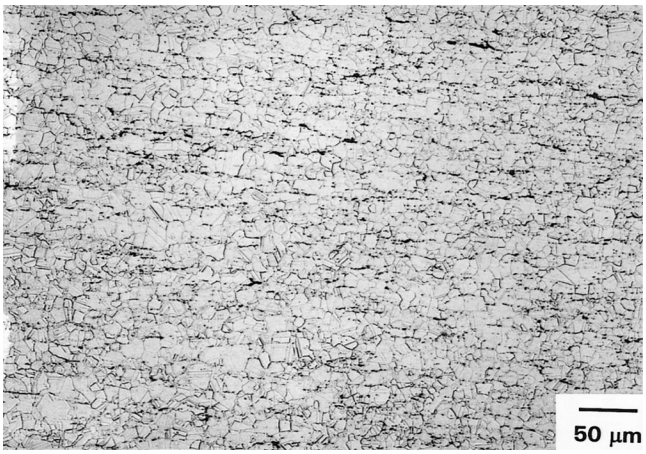

(*a*)

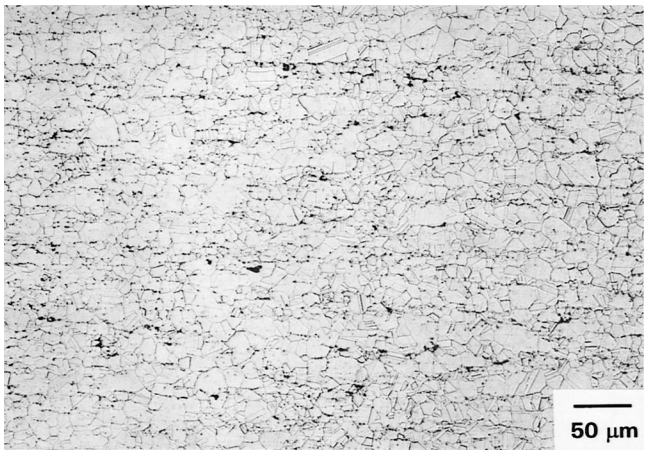

(*b*)

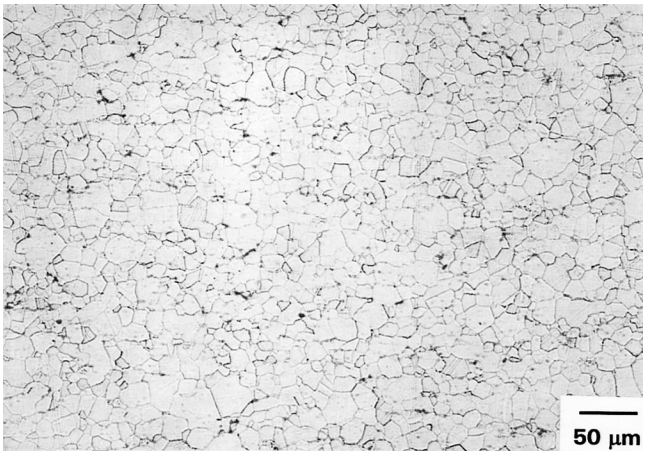

(*c*)

Fig. 6—Microstructures of IN 625 specimens deformed at a strain rate of 100/s and at temperatures of (*a*) 1100 °C, (*b*) 1150 °C, and (*c*) 1200 °C. These exhibit wavy or irregular grain boundaries typical of DRX.

is generally observed for DRX.[12] In conclusion, the higher strain rate domain may be interpreted to represent DRX of the γ phase of the material at temperatures where the δ precipitates have gone into solution. In view of the higher strain rates and higher temperatures, this domain may be exploited for bulk metal working such as high speed rolling or drop forging to manufacture semiproducts.

D. *Instability Maps*

The continuum instability criterion given by Eq. [2] suggests that the material will exhibit flow instabilities if the dimensionless parameter $\xi(\dot{\varepsilon})$ is negative. The instability criteria have been applied to develop instability maps for IN 625 on the basis of this criterion and are shown in Figures 7(a) through (d) for strains of 0.1, 0.2, 0.3, and 0.5. The contours for constant negative values of $\xi(\dot{\varepsilon})$ are shown in these figures. It may be noted that the continuum criterion given by Eq. [2] breaks down once cracking in the adiabatic shear band occurs and the $\xi(\dot{\varepsilon})$ value changes its sign sharply (seen as thick lines). These may be superimposed on the respective power dissipation maps given in Figures 3(a) through (d) in order to delineate regimes of flow instability. The criterion suggests in general that flow instabilities will occur at temperatures lower than about 1050 °C and strain rates higher than 0.1 s^{-1}. The microstructural manifestation of the flow instabilities occurring at temperatures lower than 1050 °C are shown in Figures 8(a) through (c), which correspond to specimens deformed at 900 °C/100 s^{-1}, 950/100 s^{-1}, and 900/10 s^{-1}, respectively. These microstructures exhibit adiabatic shear bands that are oriented at about 45 deg with respect to the compression axis and become very intense at 900 °C/100 s^{-1} to cause cracking along the band (Figure 8(a)). It is interesting to note that in this regime, the stress - strain curves exhibit a high rate of work hardening up to a critical strain and flow softening at larger strains (Figure 2(a)). In view of the athermal nature of the adiabatic shear band formation, the work hardening rate is not sensitive to strain rate. The regime of instability has to be avoided in processing this material.

E. *Comparison with Earlier Studies*

Processing maps, which are a superimposition of respective power dissipation maps and instability maps, have been developed on the basis of the flow stress data published by Zhao *et al.*[3] The transient features similar to those explained previously have been observed in these maps also. The map

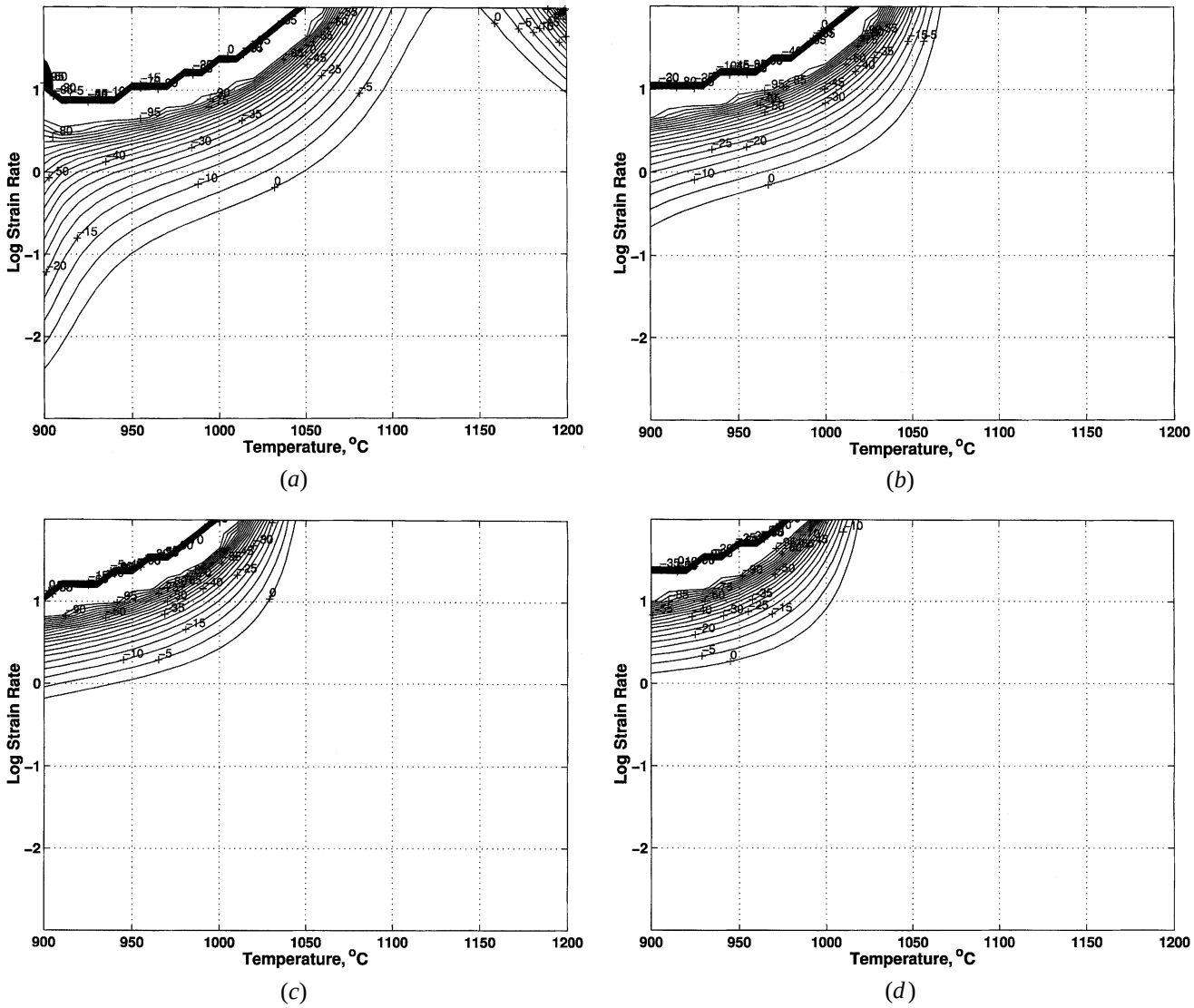

Fig. 7—Instability map obtained on IN 625 at a strain of (*a*) 0.1, (*b*) 0.2, (*c*) 0.3, and (*d*) 0.5. [The contours represent the value of the flow instability parameter $\xi(\dot{\varepsilon})$.] Flow instability is predicted to occur when $\xi(\dot{\varepsilon})$ is negative.

obtained at a strain of 0.5 is shown in Figure 9, which exhibits two domains:

(1) at temperatures lower than about 1050 °C and strain rates lower than 0.01 s^{-1} with a peak efficiency of about 45 pct occurring at about 975 °C and 0.001 s^{-1}, and
(2) at temperatures above 1100 °C and strain rates lower than 0.1 s^{-1} with a peak efficiency of about 36 pct occurring at 1150 °C and 0.01 s^{-1}.

It is obvious from the discussion in the previous sections that these two represent DRX process occurring with and without δ precipitates in the γ matrix. Also, there is a regime of flow instability due to adiabatic shear band formation at temperatures lower than about 1050 °C and strain rates higher than about 1 s^{-1}. A comparison of this map with that for the P/M IN 625 given in Figure 3(d) reveals that both DRX domains have moved to higher strain rates in the P/M alloy and that the domain of wedge cracking occurs only in the P/M material. Neither of these materials exhibit superplastic deformation. These differences may be attributed to the fact that although P/M alloys have a more uniform chemistry from location to location than cast and wrought materials, the inclusion density is greater, which will lead to a finer grain size. In particular, the fine-grained structure is well known to promote grain boundary sliding, which will result in wedge cracking and, if prevented, leads to superplastic deformation.

IV. CONCLUSIONS

On the basis of the flow stress data obtained from hot compression experiments over a temperature range of 900 °C to 1200°C and strain rate range of 0.001 to 100 s^{-1}, processing maps have been developed with a view to characterize the mechanisms of hot deformation in IN 625 P/M superalloy. The following conclusions are drawn from this investigation.

1. The stress-strain curves at strain rates lower than about 0.01 s^{-1} exhibited near steady-state flow, while at higher

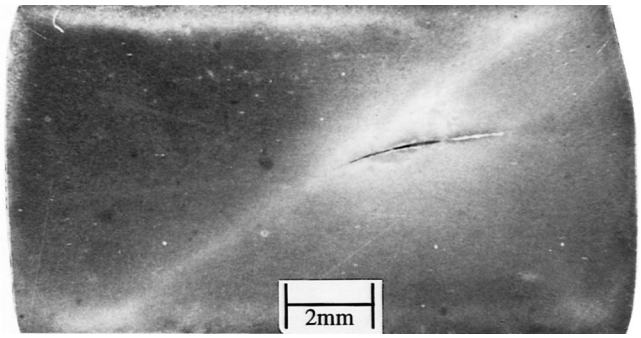

(*a*)

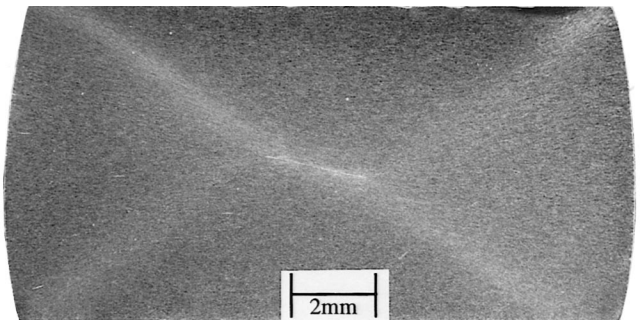

(*b*)

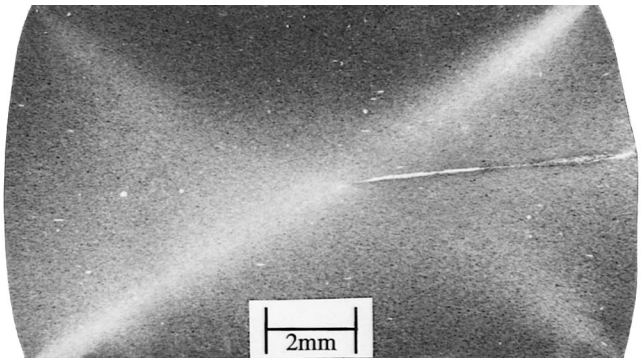

(*c*)

Fig. 8—Microstructures of IN 625 specimen deformed in the instability regime: (*a*) 900 °C and 100 s^{-1}, (*b*) 950 °C and 100 s^{-1}, and (*c*) 900 °C and 10 s^{-1}. The compression axis is vertical.

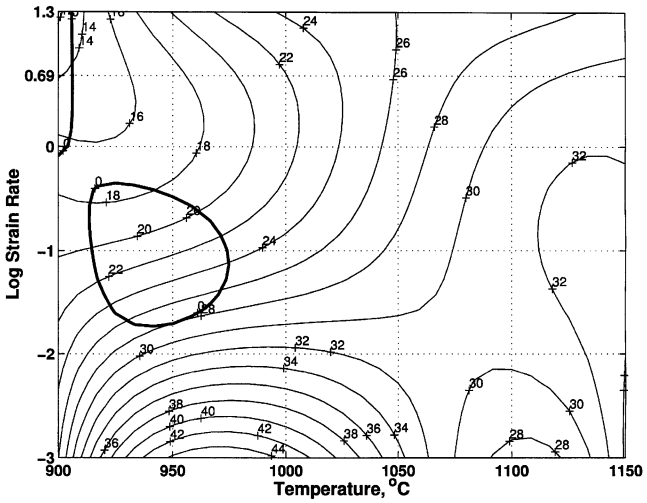

Fig. 9—Processing map obtained on Pyromet 625 from the data published by Zhao *et al.* [3] The contours represent efficiency of power dissipation in percent.

strain rates, flow stresses reached a peak before flow softening or steady, state occurred.

2. The material exhibited a domain of dynamic recrystallization at temperatures lower than about 1050 °C and in the strain rate range 0.01 to 0.1 s^{-1}, where the δ precipitates and carbide particles are present in the γ matrix. This domain is preferred for finish forming operations, where grain refinement is the objective.
3. At temperatures higher than 1050 °C and strain rates higher than 10 s^{-1}, another domain of dynamic recrystallization of γ occurs when δ precipitates go into solution. The optimum conditions for this domain are 1150 °C and 100 s^{-1}, where the characteristic efficiency of power dissipation is about 42 pct. This domain is preferred for bulk metal working of the material, since the temperature and strain rate ranges are suitable for processes such as high speed rolling or drop forging.
4. The material exhibits a domain of wedge cracking at temperatures higher than 1050 °C and strain rates lower than about 0.01 s^{-1}, and these conditions are unsuitable for any hot working operations in view of a drastic reduction in hot workability.
5. At strain rates higher than about 1 s^{-1} and temperatures below 1050 °C, intense flow instability occurs in the form of adiabatic shear band formation, and again, this regime is also to be avoided in processing this material.

ACKNOWLEDGMENTS

One of the authors (YVRKP) thanks the National Research Council (United States), for awarding him an associateship, and the Director of Indian. Institute of Science (Bangalore) for granting him a sabbatical leave. The assistance rendered by Messrs. S. Sasidhara and R. Ravi, Department of Metallurgy, Indian Institute of Science (Bangalore), is gratefully acknowledged.

REFERENCES

1. R.B. Frank and T.A. DeBold: *NACE Corrosion '88 Conf.*, St. Louis, MO, Mar. 21–25, 1988, [paper no. 75.]
2. *Alloy Data Custom Age 625 Plus Alloy*, Carpenter Technology Corporation, Reading, PA.
3. D. Zhao, P.K. Chaudhury, R.B. Frank, and L.A. Jackman: in *Superalloys 718, 625, 706 and Various Derivatives*, E.A. Loria, ed., TMS, Warrendale, PA, 1994, pp. 315-29.
4. C.R. Conger, G.D. Smith, and J.F. Radavich: in *Superalloys 718, 625, 706 and Various Derivatives*, E.A. Loria, ed., TMS, Warrendale, PA, 1997, pp. 447-58.
5. Y.V.R.K. Prasad, H.L. Gegel, S.M. Doraivelu, J.C. Malas, J.T. Morgan, K.A. Lark, and D.R. Barker: *Metall. Trans. A*, 1984, vol. 15A, pp. 1883-92.
6. *Hot Working Guide: A Compendium of Processing Maps*, [Y.V.R.K. Prasad and S. Sasidhara, eds.,], ASM INTERNATIONAL, Materials Park, OH, 1997.
7. Y.V.R.K. Prasad and T. Seshacharyulu: *Int. Mater. Rev.*, 1998, vol. 44, pp. 243-58.

8. R. Raj: *Metall. Trans. A*, 1981, vol. 12A, pp. 1089-97.
9. A.H. Chokshi, A.K. Mukherjee, and T.G. Langdon: *Mater. Sci. Eng.*, vol. R10, 1993, pp. 237-74.
10. N. Srinivasan and Y.V.R.K. Prasad: *Metall. Mater. Trans. A*, 1994, vol. 25A, pp. 2275-84.
11. S.C. Medeiros: Masters Thesis, Wright State University, Dayton, OH, 1999.
12. T. Sakai and J.J. Jonas: *Acta Metall.*, 1984, vol. 32, pp. 189-209.